A STATISTICAL INVESTIGATION OF THE LASER ENERGY ABSORPTION AND KEYHOLE STABILITY IN HIGH-POWER LASER BEAM WELDING

X. MENG*, S. PUTRA*, M. BACHMANN*, M. RETHMEIER**,*,***

**BAM Bundesanstalt für Materialforschung und -prüfung, 12205 Berlin, Germany*
***Technische Universität Berlin, Institute of Machine Tools and Factory Management, 10587 Berlin, Germany*
****Fraunhofer IPK, 10587 Berlin, Germany*

DOI 10.3217/978-3-99161-089-2-006, license CC BY 4.0

ABSTRACT

The behaviour of the weld pool in high-power laser beam welding is significantly influenced by laser absorption and keyhole stability, which determines the final weld qualities. However, their dynamic features and multi-coupled interactions make in-depth analyses difficult. This study addresses the challenges by conducting a thorough statistical evaluation of the effects of welding parameters on laser absorption and keyhole fluctuations, using experimental investigations and a well-validated numerical model. From a statistical aspect, the laser energy distribution and the keyhole collapse, commonly considered highly time-varying, show clear regularities. Three distinct regions of the time-averaged energy distribution are identified. The possibility of the keyhole collapse positions obeys a universal normal distribution. The statistical data show greater potential in revealing some well-known, industry-related but unclearly explained findings, such as the saturation of the weld penetration with increasing heat input and the physical basis of the contributions of different welding parameters in the porosity reduction.

Keywords: Laser beam welding, laser absorption, keyhole stability, multi-physics modelling

INTRODUCTION

High-power laser beam welding (LBW) has become increasingly attractive in industrial applications due to its high efficiency and precise control [1]. The most important characteristic of LBW is the formation of a narrow and deep keyhole inside the weld pool, generated by intense laser-induced evaporation. Within this keyhole, the laser beam reflects multiple times against dynamic, irregular keyhole surfaces. Although liquid metals exhibit

low direct laser absorptivity [2], the cumulative absorption from repeated reflections enables thermal efficiencies of up to 90% [3]. This absorption mechanism profoundly influences the welding process, driving melting, chemical reactions, and microstructural evolutions. However, these interactions can also lead to common defects such as spatter, hot-cracking, and porosity. Hence, deeper physical insights into laser absorption and keyhole dynamics are critical for optimizing the LBW process.

Monitoring keyhole behaviour during welding is challenging due to the opaque nature of liquid metals and rapidly evolving geometries. Techniques such as Optical Coherence Tomography (OCT) have provided transient one-dimensional measurements of the keyhole depth [4]. Alternatively, the sandwich configuration, using a metal plate and heat-resistant glass, allows a two-dimensional side view of the keyhole, captured through high-speed cameras [5]. However, detailed keyhole features, like fine surface fluctuations, are often obscured in this method due to the image overexposure. The x-ray transmission imaging technique significantly improves visualization, offering clear two-dimensional or even three-dimensional reconstruction of the transient keyhole geometry. High-quality synchrotron x-ray sources achieve micrometer-level spatial and MHz-level temporal resolution, enabling precise observation of fine structural details within keyhole dynamics [6-8].

Direct measurement of laser absorption inside the keyhole remains technically unfeasible. Consequently, indirect strategies, such as reconstructing keyhole shapes using high-speed photography [9] or x-ray radiography [10,11] followed by ray-tracing analysis, have been developed. These approaches estimate energy distribution and overall absorptivity, revealing, for instance, that approximately 40% of the laser energy is absorbed by the front keyhole wall [9].

Recently, multi-physics modelling has become an effective tool for understanding LBW phenomena. By integrating physics-based beam interaction models with interface tracking algorithms, these simulations effectively predict laser absorption and keyhole topology [12-14]. Studies using these models have identified the inclination angle of the keyhole's front wall as a crucial factor influencing absorption and energy distribution [15]. A more inclined front wall, common at higher welding speeds, tends to distribute energy uniformly. Additionally, microscopic protrusions on keyhole walls strongly influence energy absorption, driving keyhole instability and fluctuations [16,17].

However, current experimental and numerical analyses typically examine short and sometimes selective instances of the keyhole dynamics, which lack statistical robustness. Only limited research has been performed from a statistical perspective. For example, in the study of Pang et al., the keyhole depth fluctuations were found to have a normal distribution [18]. Important aspects like average laser absorption during melting or the likelihood of porosity-related keyhole collapse remain unexplored.

Addressing these gaps, this paper presents a comprehensive statistical analysis using multi-physics modelling to investigate laser energy absorption and keyhole stability over an extended duration (more than 100 ms). Statistical evaluations explore how welding parameters (welding speed and focus position) influence keyhole dynamics and energy absorption. This approach reveals novel insights into LBW physics, highlighting the advantages of statistical methods in understanding and optimizing this complex process.

METHODOLOGY

EXPERIMENTS

Bead-on-plate welding experiments were performed using 304 stainless steel plates measuring 200 mm length, 60 mm width, and 10 mm thickness. The laser source was a Trumpf disk laser system emitting at a wavelength of 1.03 μm with a focal diameter of 0.42 mm. The laser beam was vertically aligned to the plate surface. Welding parameters investigated included welding speed (1.5 m/min to 3.0 m/min) and focal position (ranging from -6 mm to +3 mm). Before welding, the steel surfaces were mechanically cleaned to remove oxide layers. Cross-sections were prepared from welded samples for further examination, involving grinding, polishing, and etching using a V2A solution. Optical microscopy was utilized to analyse these cross-sections metallographically, capturing the fusion zone profiles and measuring penetration depths to validate experimental results.

MULTI-PHYSICS MODELLING

Under the following assumptions: (1) the liquid metal behaves as an incompressible Newtonian fluid, (2) fluid flow remains laminar, and (3) buoyancy is modelled using the Boussinesq approximation, where density variations due to temperature are neglected except in buoyancy terms, the governing equations for heat transfer, fluid flow, and free surface deformation during LBW can be expressed as follows:

$$\nabla \cdot \mathbf{v} = 0 \tag{1}$$

$$\rho\left(\frac{\partial \mathbf{v}}{\partial t} + (\mathbf{v}\cdot\nabla)\mathbf{v}\right) = -\nabla p + \mu\nabla^2\mathbf{v} - \mu K\mathbf{v} + \mathbf{S_m} + \mathbf{F} \tag{2}$$

$$\rho\left[\frac{\partial h}{\partial t} + (\mathbf{v}\cdot\nabla)h\right] = \nabla\cdot(k\nabla T) + Q \tag{3}$$

$$\frac{\partial f}{\partial t} + \nabla\cdot(\mathbf{v}f) = 0 \tag{4}$$

Equation (1) represents mass conservation, where **v** is the velocity vector. Equation (2) describes momentum conservation, where ρ denotes material density, t physical time, p pressure, μ dynamic viscosity, and K the damping coefficient associated with solidification. The vector $\mathbf{S_m}$ includes various source terms such as buoyancy and gravitational forces, while **F** represents volumetric forces derived from surface phenomena [19], including capillary pressure, Marangoni stress, and recoil pressure. Equation (3) expresses energy conservation, with h as enthalpy, T temperature, k thermal conductivity, and Q the heat source term

representing converted surface energy. Equation (4) is the volume-of-fraction (VOF) equation used to track the interface, where *f* is the volume fraction of steel.

The model incorporates key factors affecting melting and keyhole dynamics. Laser heating is simulated using a physics-based beam propagation model, which will be described further in the following part. Additional heat from scattering and absorption is considered through two diffuse heat-source models [20]. Thermal losses from convection, radiation, and evaporation are applied at the interface. Capillary pressure, Marangoni stress, and temperature-dependent recoil pressure [21] are included to simulate the keyhole evolution. The stagnation pressure and shear stress generated by the vapor jet are modelled analytically using the Knudsen layer theory and the free jet theory [20] for accurate simulation of the keyhole dynamics.

Accurate modelling of beam propagation and laser-material interactions is essential for understanding laser absorption and keyhole behaviour. In this study, a ray-tracing algorithm is implemented to track the laser beam, including initial and subsequent reflections on the keyhole surface. Beam focusing or defocusing due to the caustic effect are also considered. Since the VOF method does not explicitly define the interface, reflection accuracy is typically restricted by the cell size [22]. To improve precision, a localized Level-Set (LS) approach reconstructs the keyhole interface mathematically [23], allowing the exact determination of reflection points without significantly increasing computational costs.

Commonly used laser absorption models rely on the incident angle alone, requiring empirical calibration for other physical factors [24,25]. A novel Fresnel reflection model based on the Drude–Lorentz theory [26], calculating the relative electric permittivity of metals, is employed in this study. This new model considers the incident angle, laser wavelength, surface temperature, and electrical conductivity, which eliminates the adjustment/calibration of empirical parameters.

The simulation domain consists of a 10 mm thick metallic phase and a 1 mm thick argon gas phase. The initial mesh includes a uniformly meshed central region (2 mm to 8 mm in the x-direction and -2 mm to 2 mm in the y-direction) with 0.2 mm hexahedral cells, which gradually increase in size to approximately 0.7 mm outside this region. A multi-level mesh adaptation approach is used to refine the mesh progressively from 0.2 mm to 0.1 mm and finally to 0.05 mm within the region of interest (keyhole and weld pool). ANSYS Fluent 23.1 is used to solve the governing equations. The total number of cells increases from an initial 78,000 to around 680,000 as the keyhole and weld pool evolve, as illustrated in Fig. 1. The simulations run on a high-performance computing cluster at Bundesanstalt für Materialforschung und -prüfung, where at least 10 ms of physical simulation time is achieved every 24 hours using 88 cores and 256 GB of memory.

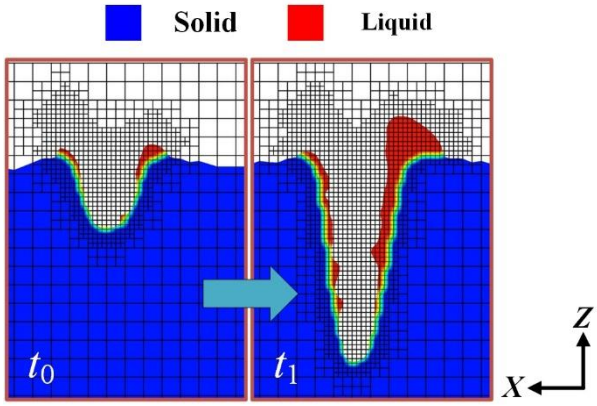

Fig. 1 The mesh refinement from the multi-level mesh adaptation

RESULTS AND DISCUSSION

Fig. 2 presents a representative validation of the simulated penetration depths across the studied welding parameter ranges in the current study. The proposed model achieves good accuracy, exhibiting minor deviations of approximately -11% to +5% compared to experimental measurements. In the following section, a detailed parametric investigation will be performed to statistically analyse the effects of welding speed and focal position on laser energy absorption and keyhole stability over an extended period of more than 100 ms.

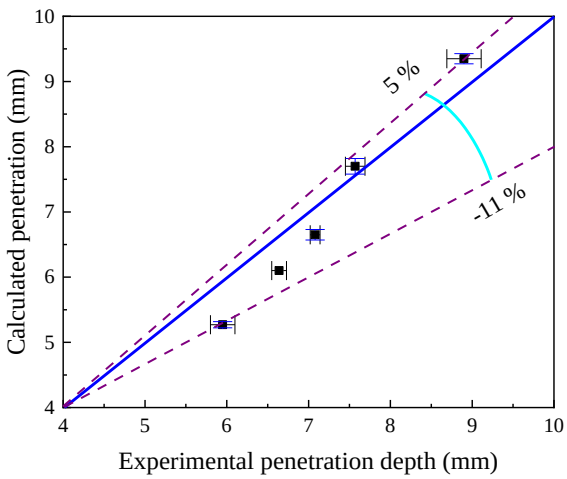

Fig. 2 Comparison between experimental and simulated penetration depths

STATISTICAL ANALYSIS OF LASER ABSORPTION

Fig. 3 illustrates the influence of welding speed on the time-averaged laser energy absorption along the longitudinal cross-section. All contours are normalized relative to the maximum power density for the respective welding conditions. A transient keyhole profile (solid black line) is included for spatial reference. At all welding speeds, the front keyhole wall consistently shows higher absorption due to the initial laser incidence. The upper region of the rear wall also absorbs a notable amount of energy. Compared with the transient laser energy density [10,11,16,17], the time-averaged laser energy exhibits a relative regular distribution regime.

To analyse the overall energy distribution along the thickness direction and the welding directions, the time-averaged power density (in W/m²) at each z-level/x-level is integrated to yield a line distribution (in W/m), which is then divided by the welding speed to obtain the averaged linear energy. As shown in Fig. 4(a), three distinct regions are observed along the thickness direction: an upper zone with intensive energy absorption, a middle region exhibiting a relatively uniform distribution, and a lower region where absorbed energy declines sharply. While the welding speed has limited influence on the general distribution shape, an inverse correlation is evident in the upper region, namely higher welding speeds correspond to reduced energy absorption. Fig. 4(b) shows the energy distribution across the front and rear keyhole walls. For clarity, the laser axis is used to separate the front and rear wall regions. Steep gradients in front of the axis indicate concentrated energy absorption on the front keyhole wall, while gentler slopes behind it reflect more gradual absorption on the rear wall. On a time-averaged basis, the absorption ratio on the front wall decreases from 37% to 30.5% as welding speed increases from 1.5 m/min to 3.0 m/min.

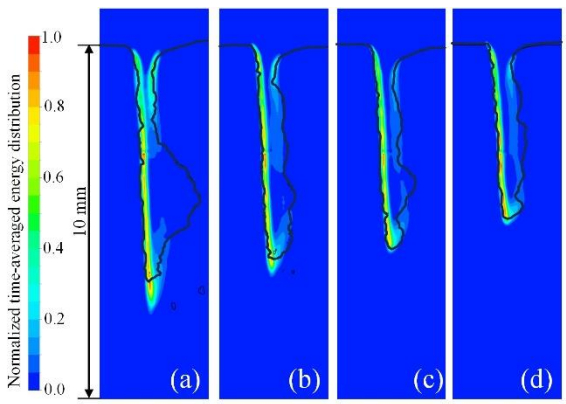

Fig. 3 The influence of welding speed on time-averaged laser absorption: (a) 1.5 m/min, (b) 2.0 m/min, (c) 2.5 m/min, (d) 3.0 m/min. (laser power: 4 kW, focal position: -3 mm)

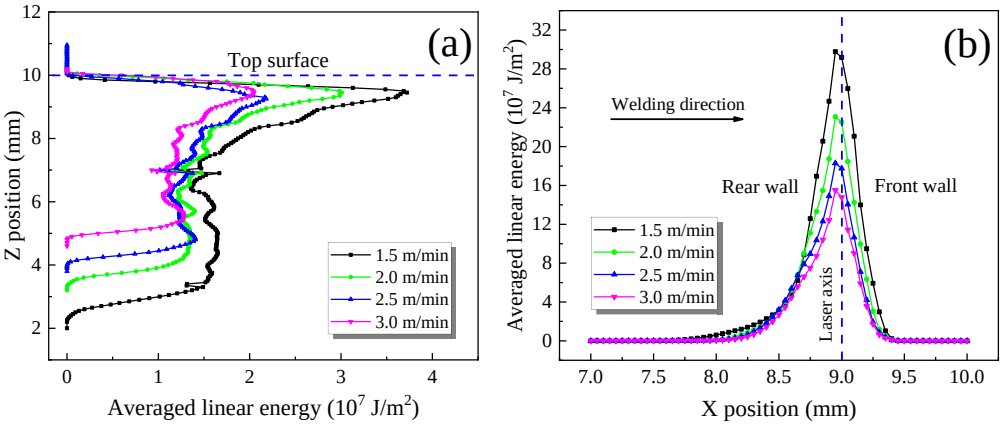

Fig. 4 Time-averaged linear energy: (a) along the thickness direction, (b) along the welding direction (laser power: 4 kW, focal position: -3 mm)

The focal position has a more pronounced impact on the pattern of laser energy distribution than the welding speed. Even with similar linear energy input, variations in focal position result in different time-averaged energy profiles, leading to different penetration depths, as shown in Fig. 5. Fig. 6 further demonstrates the significant influence of the focal position on the time-averaged energy distribution, particularly in the middle and lower regions of the keyhole. A negative focal position of -3 mm produces the deepest penetration, attributed to a stable absorption zone extending to the keyhole bottom. At focal position of -6 mm, this stable zone becomes less distinct, with a gradual reduction in absorbed energy along the depth. In contrast, with a zero or positive focal position, the absorbed energy increases slightly near the keyhole bottom rather than declining, an unusual distribution potentially associated with the formation of porosity and hot cracking [27]. Additionally, as the focus shifts from positive to negative, the absorption ratio on the front keyhole wall steadily decreases-from 40.5% to 36.8%.

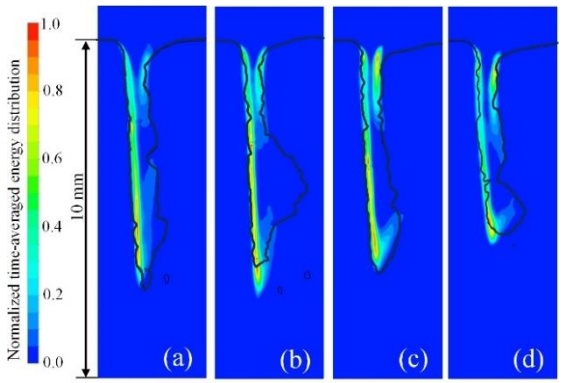

Fig. 5 The influence of focal position on the time-averaged laser absorption: (a) -6 mm, (b) -3 mm, (c) 0 mm, (d) +3 mm (Laser power: 4 kW, welding speed: 2 m/min)

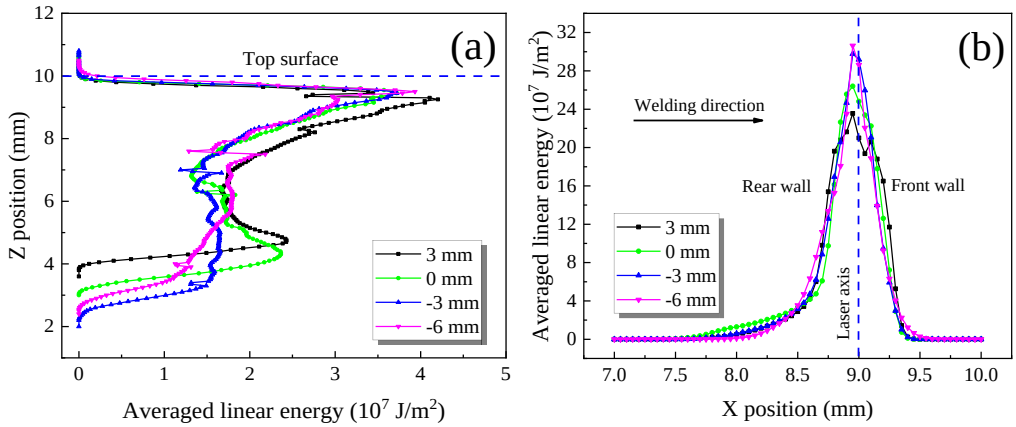

Fig. 6 Time-averaged total linear energy: (a) along the thickness direction, (b) along the welding direction

STATISTICAL ANALYSIS OF THE KEYHOLE STABILITY

To comprehensively assess keyhole stability, several indicators are considered in this study: collapse position, fluctuation frequency, and collapse duration. A collapse is defined as the moment when the front and rear keyhole walls come into contact. The location of this contact is a key metric for evaluating stability, while the number of collapses per second is defined as the fluctuation frequency. Each collapse also has a corresponding duration, measured from the initial contact to the moment when the walls separate again.

Fig. 7 presents the possibility of collapse occurrences along the keyhole depth. Most collapses occur near the keyhole tip and follow a normal distribution, aligning well with

previous findings [18,28]. Lower welding speeds, which generate deeper keyholes, are associated with broader collapse ranges. As the welding speed decreases from 3.0 m/min to 1.5 m/min, the collapse range increases from 0.7 mm to 2.0 mm, leading to larger gas bubbles and potentially more serious porosity issue. The collapse frequency remains relatively stable between 7 kHz and 8.4 kHz for welding speeds between 1.5 m/min and 2.5 m/min, but rises sharply to 180 kHz at 3.0 m/min.

Fig. 8 shows a scatter plot of individual collapse durations versus position, with each point representing a single collapse occurrence. The points are color-coded using kernel density estimation (KDE). Higher KDE values (red regions) indicate more frequent collapse behaviour in that area. It is clearly indicated that although keyhole fluctuations occur at high frequencies (from several kilohertz up to hundreds of kilohertz), most collapses are short-existing (under 1 ms) and are rapidly reopened due to a strong recoil pressure. A comparison of Fig. 8(a)-8(d) reveals that increasing welding speed significantly reduces the number of long-duration collapses. Since only collapses with extended durations are likely to form gas bubbles in the weld pool and potentially lead to porosity in the final weld, it can be expected that the reduction of the long-duration collapses will enhance the keyhole stability.

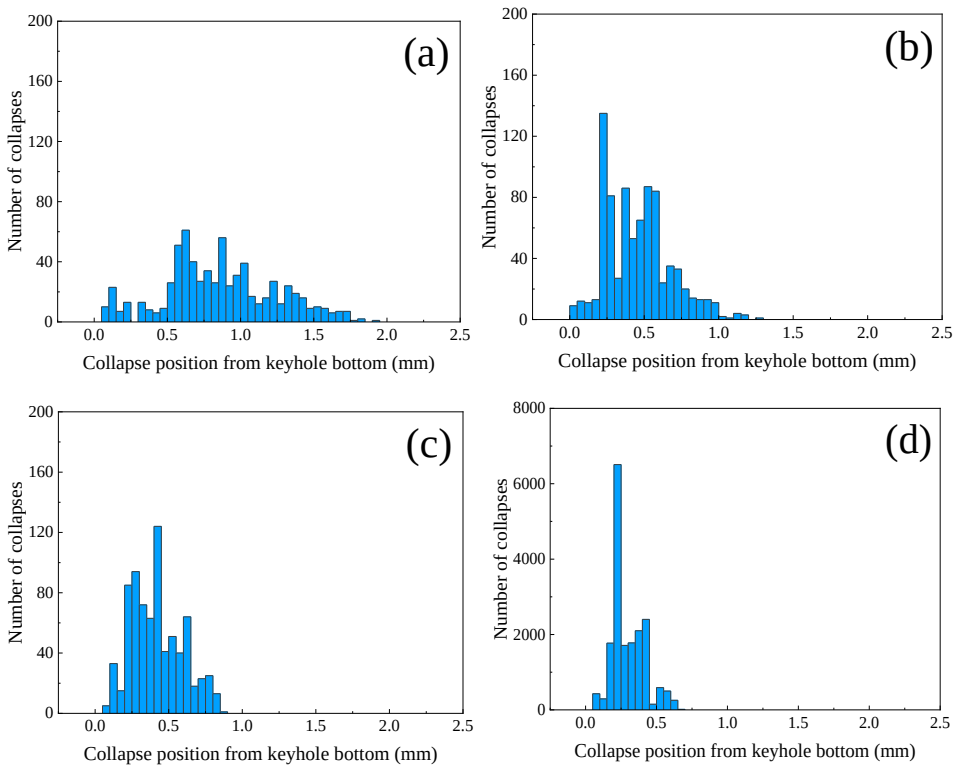

Fig. 7 The influence of welding speed on collapse number: (a) 1.5 m/min, (b) 2.0 m/min, (c) 2.5 m/min, (d) 3.0 m/min (Laser power: 4 kW Focal position: -3 mm)

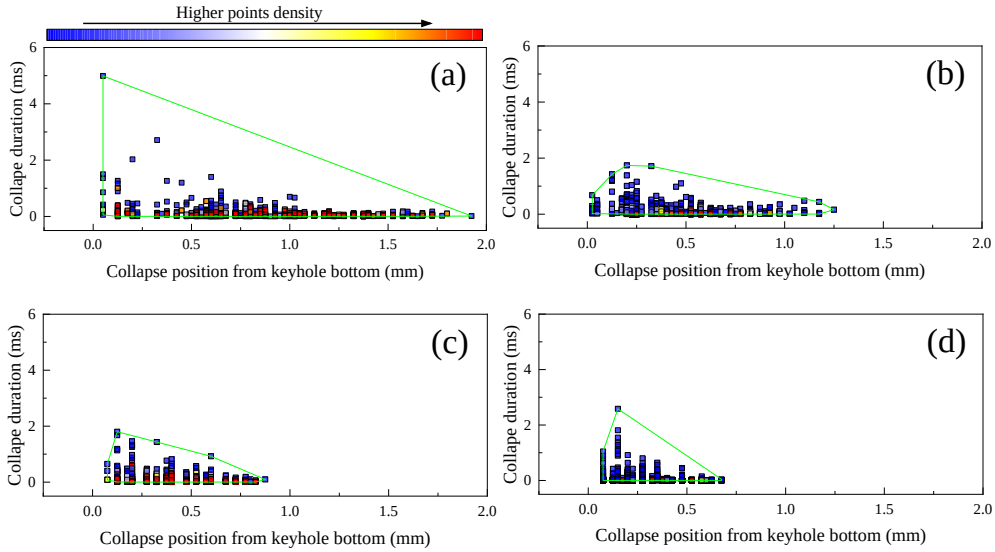

Fig. 8 Duration of individual collapse at different positions: (a) 1.5 m/min, (b) 2.0 m/min, (c) 2.5 m/min, (d) 3.0 m/min (Laser power: 4 kW Focal position: -3 mm)

Compared to welding speed, the focal position exhibits a complex influence on keyhole stability. A deeply focused beam positioned at -6 mm (relative to the workpiece surface) not only induces collapses at the keyhole bottom, which follows also a normal distribution, but also leads to occasional collapses in the upper keyhole region, as illustrated in Fig. 9(a). These upper-region collapses are typically short in duration and are expected to contribute only marginally to overall keyhole instability, as shown in Fig. 10(a). As the focal position is adjusted upward, these upper-region collapses disappear, and collapses are confined to the keyhole bottom. Fig. 9 and Fig. 10 further demonstrate that the collapse region, closely related to potential bubble size, becomes narrower, and the number of long-duration collapses decreases as the focal plane moves closer to the surface. This behaviour suggests a reduced likelihood of porosity formation at shallower focal positions.

At the same time, the collapse frequency increases from 4.8 kHz to 9.1 kHz as the focus is raised from -6 mm to +3 mm. While this rise in frequency may increase the number of collapses, which potentially contributes to porosity formation, the simultaneous reduction in collapse area and duration may counterbalance this effect. Overall, the impact of focal position on keyhole dynamics is found to be both non-linear and non-monotonic, consistent with observations reported in several experimental studies [29-31].

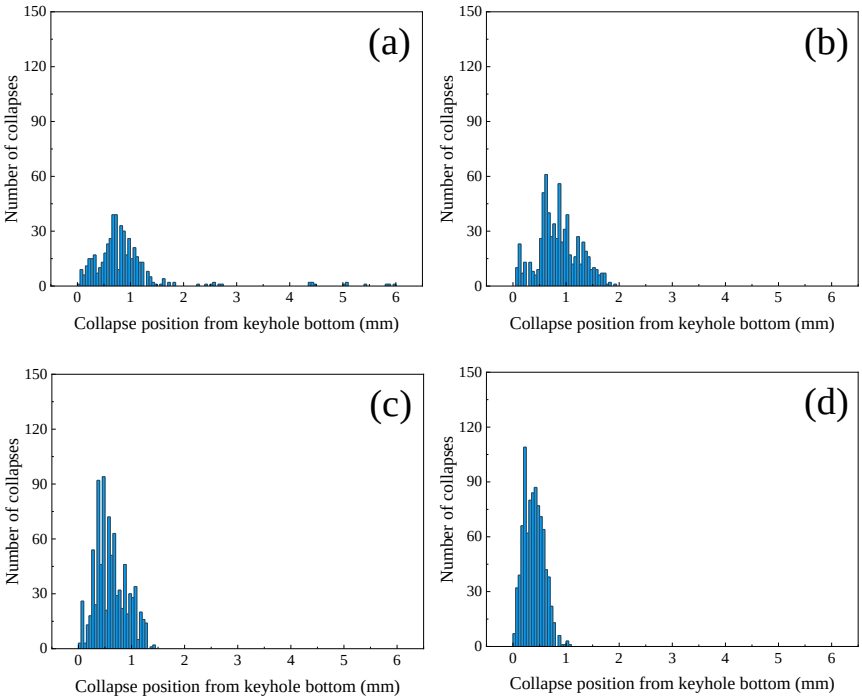

Fig. 9 The influence of focus position on collapse number: (a) -6 mm, (b) -3 mm, (c) 0 mm, (d) +3 mm (Laser power: 4 kW, welding speed: 2 m/min)

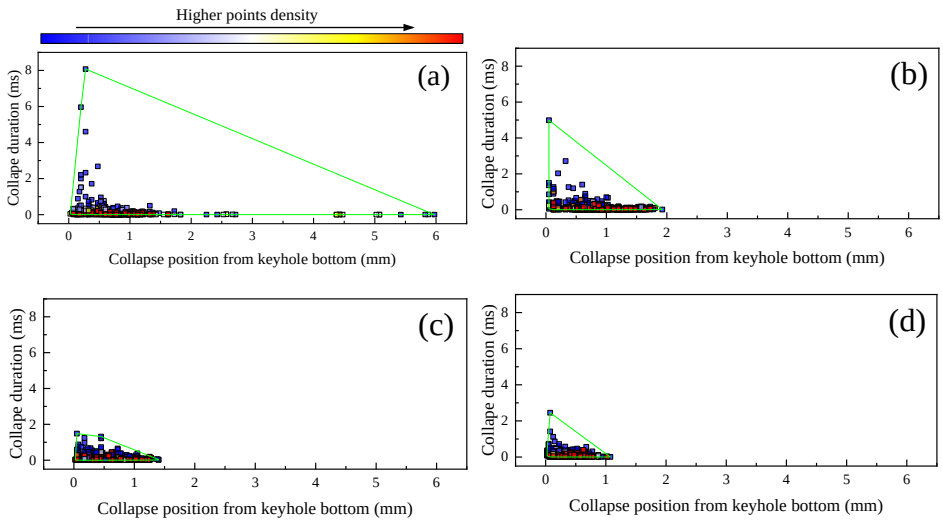

Fig. 10 Duration of individual collapse at different positions: (a) -6 mm, (b) -3 mm, (c) 0 mm, (d) +3 mm (Laser power: 4 kW, welding speed: 2 m/min)

CONCLUSION

With the integration of experimental investigation and multi-physics modelling, this paper presents a statistical evaluation of the effects of welding parameters, including welding speed and focus position, on laser energy absorption and keyhole stability in high-power LBW. The main conclusions are summarized as follows:

1. Three distinct regions of laser absorption are identified from a time-averaged perspective: an upper region with higher absorption, a middle region with relatively uniform energy intensity, and a lower region where energy absorption declines sharply. This distribution pattern is only slightly influenced by variations in welding speed whereas focus position exerts a notably stronger impact on the energy distribution.
2. On a time-averaged basis, the front keyhole wall accounts for approximately 30% to 40% of the total absorbed energy due to its intensive and localized interaction with the laser beam.
3. The majority of the keyhole collapses occur in the lower region, and their spatial distribution follows a normal distribution. Increasing welding speed is effective in narrowing the collapse zone and shortening collapse durations. The influence of focus position is found to be non-linear and non-monotonic.

ACKNOWLEDGMENT

This work is funded by the Deutsche Forschungsgemeinschaft (DFG, German Research Foundation)-Project No. 506270597 and No. 466939224.

References

[1] M. RETHMEIER, A. GUMENYUK and M. BACHMANN: 'High-power laser beam welding for thick section steels – new perspectives using electromagnetic systems', *Science and Technology of Welding and Joining*, Vol. 27, pp. 43-51, 2022.

[2] E. M. R. SILVA, W. A. MONTEIRO, W. ROSSI and M. S. F. LIMA: 'Absorption of Nd:YAG laser beam by metallic alloys', *Journal of Materials Science Letters*, Vol. 19, pp. 2095-2097, 2000.

[3] Y. KAWAHITO, N. MATSUMOTO, Y. ABE and S. KATAYAMA: 'Relationship of laser absorption to keyhole behavior in high-power fiber laser welding of stainless steel and aluminum alloy', *Journal of Materials Processing Technology*, Vol. 211, pp. 1563-1568, 2011.

[4] C. STADTER, M. SCHMOELLER, L. VON RHEIN and M. F. ZAEH: 'Real-time prediction of quality characteristics in laser beam welding using optical coherence tomography and machine learning', *Journal of Laser Applications*, Vol. 32, p. 022046, 2020.

[5] L. HUANG, P. LIU, S. ZHU, X. HUA and S. DONG: 'Experimental research on formation mechanism of porosity in magnetic-field-assisted laser welding of steel', *Journal of Manufacturing Processes*, Vol. 50, pp. 596-602, 2020.

[6] H. WANG, M. NAKANISHI and Y. KAWAHITO: 'Effects of welding speed on absorption rate in partial and full penetration welding of stainless steel with high-brightness, high-power laser', *Journal of Materials Processing Technology*, Vol. 249, pp. 193-201, 2017.

[7] R. CUNNINGHAM, C. ZHAO, N. PARAB, C. KANTZOS, J. PAUZA, K. FEZZAA and A. D. ROLLETT: 'Keyhole threshold and morphology in laser melting revealed by ultrahigh-speed X-ray imaging', *Science*, Vol. 363, pp. 849-852, 2019.

[8] J. XU, X. WANG, C. YAO, D. ZOU, R. XIONG, R. XIAO and B. ZHANG: 'A dual in-situ monitoring of multiphase dynamics during laser wire fusion process with synchrotron radiation and visible light', *Journal of Manufacturing Processes*, Vol. 131, pp. 2528-2534, 2024.

[9] R. S. MATTI and A. F. H. KAPLAN: 'Post-modelling of images from a laser-induced wavy boiling front', *Applied Surface Science*, Vol. 357, pp. 2277-2284, 2015.

[10] F. FETZER, C. HAGENLOCHER, R. WEBER and T. GRAF: 'Geometry and stability of the capillary during deep-penetration laser welding of AlMgSi at high feed rates', *Optics & Laser Technology*, Vol. 133, p. 106562, 2021.

[11] B. J. SIMONDS, J. TANNER, A. ARTUSIO-GLIMPSE, P. A. WILLIAMS, N. PARAB, C. ZHAO and T. SUN: 'The causal relationship between melt-pool geometry and energy absorption measured in real time during laser-based manufacturing', *Applied Materials Today*, Vol. 23, p. 101049, 2021.

[12] W. E. ALPHONSO, M. BAIER, S. CARMIGNATO, J. H. HATTEL and M. BAYAT: 'On the possibility of doing reduced-order thermo-fluid modelling of laser powder-bed fusion (L-PBF) – assessment of the importance of recoil pressure and surface tension', *Journal of Manufacturing Processes*, Vol. 94, pp. 564-577, 2023.

[13] A. OTTO, H. KOCH, K. H. LEITZ and M. SCHMIDT: 'Numerical simulations – a versatile approach for better understanding dynamics in laser material processing', *Physics Procedia*, Vol. 12, pp. 11-20, 2011.

[14] M. COURTOIS, M. CARIN, P. LE MASSON, S. GAIED and M. BALABANE: 'A new approach to compute multi-reflections of a laser beam in a keyhole for heat-transfer and fluid-flow modelling in laser welding', *Journal of Physics D: Applied Physics*, Vol. 46, p. 505305, 2013.

[15] W. TAN and Y. C. SHIN: 'Analysis of multi-phase interaction and its effects on keyhole dynamics with a multi-physics numerical model', *Journal of Physics D: Applied Physics*, Vol. 47, p. 345501, 2014.

[16] Y. WANG, P. JIANG, J. ZHAO and S. GENG: 'Effects of energy-density attenuation on the stability of keyhole and molten pool during deep-penetration laser welding: a combined numerical and experimental study', *International Journal of Heat and Mass Transfer*, Vol. 176, p. 121410, 2021.

[17] C. ZHAO, Q. GUO, X. LI, N. PARAB, K. FEZZAA, W. TAN and T. SUN: 'Bulk-explosion-induced metal spattering during laser processing', *Physical Review X*, Vol. 9, No. 2, p. 021052, 2019.

[18] S. PANG, W. CHEN and W. WANG: 'A quantitative model of keyhole-instability-induced porosity in laser welding of titanium alloy', *Metallurgical and Materials Transactions A*, Vol. 45, pp. 2808-2818, 2014.

[19] J. U. BRACKBILL, D. B. KOTHE and C. ZEMACH: 'A continuum method for modeling surface tension', *Journal of Computational Physics*, Vol. 100, No. 2, pp. 335-354, 1992.

[20] X. MENG, S. N. PUTRA, M. BACHMANN, F. YANG, A. ARTINOV and M. RETHMEIER: 'A fundamental study of physical mechanisms of wineglass-shaped fusion-zone profile in laser melting', *Journal of Materials Processing Technology*, Vol. 324, p. 118265, 2024.

[21] V. SEMAK and A. MATSUNAWA: 'The role of recoil pressure in energy balance during laser materials processing', *Journal of Physics D: Applied Physics*, Vol. 30, p. 2541, 1997.

[22] J. H. CHO and S. J. NA: 'Implementation of real-time multiple reflection and Fresnel absorption of a laser beam in a keyhole', *Journal of Physics D: Applied Physics*, Vol. 39, p. 5372, 2006.

[23] D. L. SUN and W. Q. TAO: 'A coupled volume-of-fluid and level-set (VOSET) method for computing incompressible two-phase flows', *International Journal of Heat and Mass Transfer*, Vol. 53, pp. 645-655, 2010.

[24] W. I. CHO, S. J. NA, C. THOMY and F. VOLLERTSEN: 'Numerical simulation of molten-pool dynamics in high-power disk-laser welding', *Journal of Materials Processing Technology*, Vol. 212, pp. 262-275, 2012.

[25] S. PANG, L. CHEN, J. ZHOU, Y. YIN and T. CHEN: 'A three-dimensional sharp-interface model for self-consistent keyhole and weld-pool dynamics in deep-penetration laser welding', *Journal of Physics D: Applied Physics*, Vol. 44, p. 025301, 2010.

[26] A. EBRAHIMI, M. SATTARI, S. J. BREMER, M. LUCKABAUER, G. W. R. RÖMER, I. M. RICHARDSON and M. J. HERMANS: 'The influence of laser characteristics on internal-flow behaviour in laser melting of metallic substrates', *Materials & Design*, Vol. 214, p. 110385, 2022.

[27] A. ARTINOV, X. MENG, M. BACHMANN and M. RETHMEIER: 'Study on the transition behavior of the bulging effect during deep-penetration laser beam welding', *International Journal of Heat and Mass Transfer*, Vol. 184, p. 122171, 2022.

[28] S. A. KHAIRALLAH, T. SUN and B. J. SIMONDS: 'Onset of periodic oscillations as a precursor of a transition to pore-generating turbulence in laser melting', *Additive Manufacturing Letters*, Vol. 1, p. 100002, 2021.

[29] N. SETO, S. KATAYAMA and A. MATSUNAWA: 'Porosity-formation mechanism and reduction method in CO_2-laser welding of stainless steel', *Welding International*, Vol. 16, pp. 451-460, 2002.

[30] J. S. KIM, T. WATANABE and Y. YOSHIDA: 'Effect of the beam-defocusing characteristics on porosity formation in laser welding', *Journal of Materials Science Letters*, Vol. 14, pp. 1624-1626, 1995.

[31] J. D. TUCKER, T. K. NOLAN, A. J. MARTIN and G. A. YOUNG: 'Effect of travel speed and beam focus on porosity in alloy 690 laser welds', *JOM*, Vol. 64, pp. 1409-1417, 2012.